Published May 31, 2019

Original Research

Core Ideas

- Coatings determine the cation exchange capacity (CEC) of macropore surfaces.
- We predicted the millimeter-scale, 2D spatial distribution of CEC at intact macropores.
- The approach combined infrared spectroscopy and CEC measurements of small samples.
- The CEC distribution in clay–organic coatings was similar for two different Bt horizons.

Determining Millimeter-Scale Maps of Cation Exchange Capacity at Macropore Surfaces in Bt Horizons

Martin Leue,* Steffen Beck-Broichsitter, Vincent J.M.N.L. Felde, and Horst H. Gerke

During preferential flow in structured soils, solute transport is largely restricted to a complex network of macropores. Clay–organic coatings of macropore surfaces determine soil physicochemical properties relevant for mass transport and carbon and nutrient turnover, such as the cation exchange capacity (CEC). However, due to the lack of an appropriate measurement approach, the small-scale spatial distributions of the CEC and its quantities are unknown to date. The objective of this work was to develop a method for predicting the millimeter- to centimeter-scale, two-dimensional spatial distribution of the CEC at intact macropore surfaces. Diffuse reflectance infrared Fourier transform (DRIFT) spectroscopy was used to analyze bulk soil and separated coating material and for intact macropore surfaces as DRIFT mapping. To determine effective CEC (CEC_{eff}), a reduction of soil mass down to 0.5 g for use in the standard barium chloride batch method was tested to account for the limited amount of soil material that can be separated from thin macropore coatings. Linear and partial least squares regression analyses were applied to predict the CEC_{eff} distribution at intact macropore surfaces for samples from Luvisol Bt horizons from loess (L) and glacial till (T) using DRIFT spectral data. The highest CEC_{eff} values were found for coatings and pinhole fillings rich of clay–organic material (L: 38 cmol kg^{-1}; T: 29 cmol kg^{-1}) compared with low CEC_{eff} values of uncoated cracks and earthworm burrows that were similar to those of bulk soil (L: 21 cmol kg^{-1}; T: 14 cmol kg^{-1}). The location of millimeter- to centimeter-sized regions with increased CEC_{eff} levels at intact macropore surfaces corresponded with the location of clay–organic coatings. The proposed method allows determining the CEC at macropore surfaces to quantify their effect on nutrient transport by preferential flow as well as on plant nutrient supply in macropores that may serve as preferential growth paths for plant roots.

Abbreviations: CEC, cation exchange capacity; CEC_{eff}, effective cation exchange capacity; DRIFT, diffuse reflectance infrared Fourier transform; EB, earthworm burrow; EBcast, earthworm casts; IR, infrared; L, loess; PIN, pinhole filling; PLSR, partial least squares regression; SOC, soil organic carbon; SOM, soil organic matter; T, glacial till; WN, wave number.

M. Leue, S. Beck-Broichsitter, and H.H. Gerke, Research Area 1 Landscape Functioning, Working Group Hydropedology, Leibniz Centre for Agricultural Landscape Research (ZALF), Eberswalder Straße 84, 15374 Müncheberg, Germany; V.J.M.N.L. Felde, Faculty of Organic Agricultural Sciences, Dep. of Soil Science, Univ. of Kassel, Nordbahnhofstr. 1a, 37213 Witzenhausen, Germany. *Corresponding author (Martin.Leue@zalf.de).

Received 26 Aug. 2018.
Accepted 21 Feb. 2019.

Citation: Leue, M., S. Beck-Broichsitter, V.J.M.N.L. Felde, and H.H. Gerke. 2019. Determining millimeter-scale maps of cation exchange capacity at macropore surfaces in Bt horizons. Vadose Zone J. 18:180162. doi:10.2136/vzj2018.08.0162

In structured soils, macropores (e.g., biopores, root channels, shrinkage cracks, and interaggregate spaces) can serve as preferential flow paths (Alaoui et al., 2011; Jarvis, 2007). During preferential flow events, macropore surfaces act as interfaces between macropores and the porous soil matrix but also as "hot spots" of nutrient and C turnover (Abou Najm et al., 2010; Bundt et al., 2001; Kuzyakov and Blagodatskaya, 2015). The bio-physicochemical properties of macropore surfaces, such as the wettability of root channels, cracks, and earthworm burrow (EB) walls (Leue et al., 2015), and the hydraulic conductivity (Fér et al., 2016; Gerke and Köhne, 2002) can differ from that of the soil matrix due to coatings of clay–organic material. These coatings are particularly distinctive along EBs because earthworms are known to strongly influence biopore properties (Pagenkemper et al., 2015) as well as along cracks of Luvisol Bt horizons (Leue et al., 2018). In the case of wettability, the properties of the outermost nanometers of soil particles determine whether a surface is water repellent or not (Woche et al., 2017).

It can be assumed that enrichments of clay- and organic-rich material along macropore surfaces increase the cation exchange capacity (CEC) because clay minerals and soil organic

matter (SOM) are known as the most relevant soil components determining the CEC. Thus, in structured soils, the abundance and accessibility of cation adsorption sites are determined by the spatial distribution of macropore coatings and of the macropores themselves (Keck et al., 2017; Ludwig et al., 2005). In particular, when considering root growth in macropores (Kautz, 2015; Ruiz et al., 2015), preferential flow, and solute transport, the CEC of macropore surfaces is of crucial interest. Such differences in local (i.e., millimeter–centimeter scaled) distribution of the CEC cannot be represented by horizon-related measurements using bulk samples.

As a standard parameter of soil fertility, the CEC as a measure for all negatively charged sites on soil components is often determined as effective CEC (CEC_{eff}) under consideration of the soil pH. The standard $BaCl_2$ method for bulk samples uses sample masses between 2.5 and 5 g (e.g., Blakemore et al., 1987; Jaremko and Kalembasa, 2014; ISO, 2018). However, macropore coatings are thin, and thus only relatively small amounts can be obtained by manual separation of the outermost macropore surface (Leue et al., 2016, 2018). A separation of soil masses up to 2.5 g (which is the required amount for the standard analysis according to the ISO, 2018) from macropore surfaces would require the sampling of large areas of intact macropore surfaces and thus would not allow characterizing the CEC distribution at a millimeter to centimeter spatial resolution. Smaller sample amounts representing specific intact surface areas would, however, pose a great challenge to the application of the standard CEC_{eff} method.

The infrared (IR) spectroscopy in the mid-IR wavelength has been found useful to predict CEC among other chemical properties of soils (e.g., Viscarra Rossel et al., 2006), often via the application of partial least squares regression (PLSR) (e.g., Janik et al., 1998; Madari et al., 2006). Applied as diffuse reflectance infrared Fourier transform (DRIFT) spectroscopy, the technique is able to characterize the millimeter-scale, two-dimensional spatial distribution (DRIFT mapping) of SOM composition (Leue et al., 2010b, 2017), soil organic carbon (SOC) (Leue et al., 2018), and related physicochemical properties, such as wettability (Leue et al., 2015), along intact macropore surfaces. Likewise, the spatial prediction of CEC using DRIFT mapping spectra seems possible, although it requires calibration of the spectral information. In the calibration step, DRIFT data obtained from samples or sample surface areas are statistically related to physicochemical properties, such as the CEC of these samples (or surface areas) measured by a complemental approach, such as laboratory analyses of exchangeable cation contents in extraction solutions. For these relations, either entire spectra or specific signals can be used. Whereas the latter are easy to handle in a conventional linear regression (single signal intensity vs. CEC value), the former needs more sophisticated statistical methods, such as PSLR (spectrum vs. CEC value), resulting from the complex information included in the spectra (i.e., up to 3600 data points per spectrum). The obtained relationship (regression function) can then be used to predict the specific physicochemical property (CEC) of other samples or surface areas of similar origin from more easily measured DRIFT spectra or single infrared signal intensities.

As significant advantages, the DRIFT mapping technique is nondestructive (thus leaving intact the relatively thin and vulnerable macropore coatings), low cost (no additional consumables), and fast (providing large numbers of measurements in a relatively short time). Thus, it may be useful for the prediction of physicochemical macropore surface properties. However, with respect to small-scale spatial analyses, the evaluation of this approach is restricted by the limited sample masses required for complementary laboratory techniques, in particular for soil CEC determination. To obtain these sample quantities from coatings, a relatively large surface area needs to be separated if only the outermost surface (i.e., that which is exposed to the IR beam) is to be considered. Thus, any approach must consider the spatial resolution of the DRIFT mapping and of the complemental measurement approach.

The objective of this work was to develop a method for predicting the millimeter-scale, two-dimensional spatial distribution of the CEC_{eff} at intact macropore surfaces. For this purpose, we adopted the standard CEC_{eff} measurement method by systematically reducing the masses of soil material used for the CEC_{eff} determination. Linear regressions and PLSR between the CEC_{eff} of small amounts of separated surface material and DRIFT spectra of the same samples were used to exemplarily predict the millimeter-scale spatial distribution of the CEC_{eff} along intact macropore surfaces of two Luvisol Bt horizons with different textures.

Material and Methods

Soils and Sampling

Soil samples were collected from Haplic Luvisols (IUSS Working Group WRB, 2006) of arable soils, one developed from loess (L) located in northern Bohemia (Hnevceves, near Hradec Kralove, Czech Republic; 15°43′3″ E, 50°18′47″ N; mean annual precipitation, 618 mm; mean annual temperature, 8.5°C; Table 1) and one developed from glacial till (T) in northeastern Germany (Holzendorf, near Prenzlau, Uckermark region; 13°47′11″ E, 53°22′45″ N; mean annual precipitation, 501 mm; mean annual temperature, 8.7°C).

At each site, one soil pit was excavated, and six larger soil blocks of ~15-cm height, 20-cm length, and 30-cm width were cut out of the Bt horizon using a spade. Additionally, bulk samples of ~200 g were collected from all horizons (loess: Ap1, Ap2, Bt1, Bt2, Bt-Cv, Cv; glacial till: Ap1, Ap2, Bt, Cv). In the laboratory, three smaller subsamples (i.e., smaller clods of about 5–10-cm edge length) were manually separated from the larger soil blocks of each site to obtain intact crack and biopore surfaces. From these smaller soil clods, two sample sets (Sample Sets 1 and 2) were prepared as follows: (i) From a subset of two exemplarily soil clods (one per site) showing smooth crack surfaces with embedded EBs (which were difficult to find in this combination and to prepare without destruction), soil material was scraped off from the lower side of the samples with a knife to reduce the sample thickness to a

Table 1. General site information and soil horizon properties of the loess (Hnevceves) and glacial till (Holzendorf) Haplic Luvisols; mean values of three replicates are shown.

Horizon	Depth	Clay	Silt	Sand	Soil organic C
	cm	% (w/w)			
		Loess			
Ap1	0–25	18.2	66.5	15.2	1.05
Ap2	25–34	21.5	39.6	38.9	0.66
Bt1	34–57	29.4	61.4	9.2	0.48
Bt2	57–85	27.0	69.2	3.8	0.28
Bt-Cv	85–96	25.6	70.0	4.4	n.d.†
Cv	≥96	22.5	72.4	5.1	0.20
		Glacial till			
Ap1	0–25	9.6	29.4	60.9	0.82
Ap2	25–38	12.4	25.7	61.9	0.64
Bt	38–60	20.5	24.9	54.6	0.34
Cv	≥68	13.9	26.3	59.8	0.15

† Not determined.

maximum of 15 mm, leaving the macropore surfaces at the top of the samples intact. These samples with intact macropore surfaces were fixed on aluminum plates (2-mm thickness). The maximum sample dimensions were determined by the sample holder in the *xy*-positioning table in the DRIFT device (length, 120 mm; width, 80 mm; height, 17 mm). (ii) From the rest of the clods (n = 15 per site), the outermost layer (<1 mm) was manually separated from the underlying soil matrix. The macropore surfaces were classified by visual inspection as: uncoated cracks (CS) (bright crack surfaces without visible coatings), crack coatings (CS+C) (dark brown color); pinhole fillings (PIN), clay–organic material of tapped blind holes, EBs, and earthworm casts (EBcast) (Leue et al., 2018).

The bulk samples from each soil horizon of the two sites were denoted as Sample Set 3. All samples were dried over silica gel in a desiccator.

Diffuse Reflectance Infrared Fourier Transform Spectroscopy

For standard DRIFT spectral analyses, which were performed before the CEC_{eff} analyses, the soil material separated from the macropore surfaces (biopores, cracks; Sample Set 2) and the mixed samples of the soil horizons (Sample Set 3) were carefully crushed (i.e., with very low pressure) in an agate mortar without destroying the mineral soil particles (quartz grains). The undiluted soil material was poured into standard cups for DRIFT measurements in five laboratory repetitions per sample.

For the DRIFT mapping of intact sample surfaces (Sample Set 1), the aluminum plates with the fixed samples of ~1.5-cm thickness were installed in an *xy*-positioning table coupled with a DRIFT device (Pike, adapted by Resultec), which was installed in a Biorad FTS 135 spectrometer (Biorad Corp.). The DRIFT measurements were performed in 1- by 1-mm grids for one intact aggregate surface from the loess-Bt and one from the till-Bt in regions of 37 by 56 mm (L) and 60 by 100 mm (T) in *xy* dimensions (DRIFT mapping). The focus of the DRIFT device was adjusted for the average surface elevation of each sample.

For each spectrum obtained either by standard DRIFT (cups; Sample Sets 2 and 3) or DRIFT mapping (intact surfaces; Sample Set 1) technique, 16 co-added scans between wave numbers (WNs) of 4000 and 400 cm^{-1} were taken at a spectral resolution of 4 cm^{-1} and corrected for ambient air using a background spectrum of a gold target (99%; Infragold). The spectra were converted to Kubelka–Munk (KM) units, smoothed (boxcar, factor 25), and corrected for baseline shifts using the software Win-IR Pro 3.4 (Digilab). From the standard DRIFT measurements (cups; Sample Sets 2 and 3), the average spectra of the five measurement repetitions (i.e., of five spectra) were calculated using the average module of Win-IR Pro to relate these spectra to the corresponding CEC_{eff} data. For each individual spectrum, the DRIFT signal intensities (heights) were normalized against (i.e., divided by) the area of the DRIFT spectrum between WN 4000 and 400 cm^{-1} to compensate for particle size effects (Leue et al., 2010a).

Cation Exchange Capacity Laboratory Analyses and Sample Mass Calibration

The CEC_{eff}, including the exchangeable cations Na^+, K^+, Ca^{2+}, and Mg^{2+}, of the bulk samples from separated macropore surface material and the soil horizons (Sample Sets 2 and 3) was determined by the barium chloride batch method according to the ISO (2018) in three laboratory replicates. In this well-established standard method (e.g., Barton and Karathanasis, 1997; Blakemore et al., 1987), a solution of 30 mL of $BaCl_2$ is used to extract exchangeable cations from a disturbed soil sample filled in a tube or bottle. The extraction procedure is successively repeated three times to maximize extraction efficiency.

In case of bulk samples from soil horizons, the standard mass of 2.5 g soil was used per measurement. Because the separation of the macropore surfaces yielded only sample masses between 1 and 4 g in total, the standard procedure could not be applied in three sample repetitions. Thus, in two calibration tests (Calibration Tests A and B), the sample masses were methodically reduced using bulk soil material from the loess Bt horizon to evaluate the suitability of the batch method for sample masses <2.5 g.

In Calibration Test A, constant $BaCl_2$ solution volumes were used, and the sample masses were reduced stepwise to obtain decreasing soil/solution ratios as 2.5, 2.0, 1.5, 1.0, 0.8, 0.6, 0.4, 0.2, and 0.1 g soil samples. In Calibration Test B, the $BaCl_2$ solution volumes decreased proportionally to the sample masses of 2.5, 2.0, 1.5, 1.0, and 0.5 g to obtain constant soil/solution ratios. For Calibration Test B, sample masses <0.5 g could not be tested because of limitations in the available standard laboratory equipment (i.e., tubes, funnels, filters). For example, when using 0.3 g soil, most of the $BaCl_2$ solution of 3 mL is lost during the decantation steps.

Using the evaluated minimum sample mass of 0.5 g, the CEC_{eff} was determined in the bulk samples obtained from the

horizons of both Luvisols (Sample Set 3; L: $n = 6$, T: $n = 4$) and for the soil material separated from the macropore surfaces of the Bt horizons (Sample Set 2; $n = 5$ for each Luvisol-Bt). The total sum of samples was $n = 20$ (Table 2); each sample was measured in three laboratory repetitions.

pH Measurements

The pH values of bulk samples from the soil horizons (Sample Set 3; $n = 10$) and separated material from macropore surfaces (Sample Set 2; $n = 10$) of the Bt horizons were measured in each of three laboratory repetitions because pH is an important standard parameter complemental to the determination of CEC_{eff}. A 0.01 M $CaCl_2$ solution and a Mettler Toledo FE20/EL20 device with an electrode of <250 MΩ membrane resistance were used at 25°C. A pH calibration test was conducted using loess-Bt bulk samples to check the suitability of pH measurements for small soil samples. Using a constant soil/solution ratio of 1:5, the $CaCl_2$ volume decreased proportionally to sample masses of 10, 5, 1.0, 0.5, 0.1, 0.05, and 0.01 g (three repetitions each). The pH values of the soil suspension were measured in 5-mL safe-lock micro test tubes, which were only slightly thicker than the outer diameter of the electrode. Thus, the membrane of the electrode was covered already by relatively small solution volumes (minimum 0.05 mL). The pH values of the separated and bulk soil samples were finally determined from suspensions of each 0.1 g soil sample and 0.5 mL of $CaCl_2$ (three repetitions).

Table 2. Effective cation exchange capacity (CEC_{eff}) and pH of bulk soil samples from the Luvisols and of separated macropore surface material from the Bt horizons. Mean values and standard deviations (in parentheses). Ratio to B1 is the ratio between the CEC of the specific sample to the CEC of the Bt1 (loess) or Bt horizon (glacial till) of the respective Luvisol.

No.	Sample†	CEC_{eff}	CEC/Bt1	pH ($CaCl_2$)
		cmol kg^{-1}		
		Loess, bulk soil (horizons)		
1	Ap1	16.79 (0.63)	0.72	6.45 (0.02)
2	Ap2	16.51 (0.14)	0.71	6.35 (0.02)
3	Bt1	23.21 (0.63)	1.00	6.58 (0.03)
4	Bt2	21.33 (1.00)	0.92	6.62 (0.02)
5	Bt-Cv	20.50 (0.90)	0.88	6.85 (0.04)
6	Cv	18.32 (0.39)	0.79	7.63 (0.03)
		Loess, macropore surfaces Bt1 horizon		
7	CS	18.84 (0.25)	0.81	7.55 (0.03)
8	CS+C	22.58 (1.07)	0.97	6.68 (0.08)
9	PIN	37.84 (0.48)	1.63	6.52 (0.02)
10	EB	19.68 (0.31)	0.85	7.28 (0.04)
11	EBcast	18.45 (1.29)	0.79	6.50 (0.02)
		Glacial till, bulk soil (horizons)		
12	Ap1	11.15 (0.21)	0.78	7.30 (0.02)
13	Ap2	11.41 (0.20)	0.80	7.28 (0.05)
14	Bt	14.30 (0.86)	1.00	7.05 (0.07)
15	Cv	10.55 (0.51)	0.74	7.67 (0.06)
		Glacial till, macropore surfaces Bt horizon		
16	CS	10.82 (0.99)	0.76	7.42 (0.04)
17	CS+C	15.36 (0.35)	1.07	7.03 (0.05)
18	PIN	28.58 (1.25)	2.00	7.01 (0.02)
19	EB	10.01 (1.61)	0.70	7.32 (0.02)
20	EBcast	11.41 (0.75)	0.80	7.26 (0.02)

† PIN, pinhole filling; EB, earthworm burrow; EBcast, earthworm casts.

Statistical Analyses

The PLSR (Janik et al., 1998; Madari et al., 2006) between the normalized DRIFT spectra and the CEC_{eff} and pH values were performed using R, Version 3.1.1 (R Core Team, 2014) with module partial least squares (SIMPLS, cross-validation: leave-one-out). The number of components used in the calibration models depended on the lowest predicted RMSE for the respective components. We used a PLSR model of nine components, considering the entire data set of 20 samples (bulk soil and separated material from macropore surfaces). The scores and loadings were plotted for the two first components explaining most of the variances in the CEC_{eff} data. The PLSR model was used for predicting the spatial distribution of CEC_{eff} at intact sample surfaces using DRIFT mapping spectra obtained from these surfaces.

As a methodological comparison to PLSR, the DRIFT signal intensity at WN 1246 cm^{-1} was calibrated to the CEC_{eff} values as linear regression. This specific signal was identified by a linear correlation (Spearman) between the CEC_{eff} values of the bulk samples from the Luvisol horizons ($n = 10$) and the normalized signal intensities of each WN in the corresponding spectra. The WN 1246 cm^{-1} was found among the signal intensities of the highest positive correlation with the CEC_{eff} values (data not shown). It is located at a slope between peaks at WN 1160 cm^{-1}, assigned to Si–O stretching of silicates, and in the WN region 1353 to 1328 cm^{-1}, assigned to C=O, O–H, and N–O signals of SOM. A linear regression between CEC_{eff} values of the samples and the DRIFT signal intensity at WN 1246 cm^{-1} was used for predicting the spatial distribution of CEC_{eff} at intact sample surfaces using the DRIFT mapping spectra.

For validation of the calibrations, DRIFT spectra from one site were used in the PLSR model or linear regression (WN 1246 cm^{-1}) of the other site. For example, the PLSR model for the loess samples (Table 3, no. III) was used to predict the CEC_{eff} values of the till samples. These predicted CEC_{eff} values were related to the measured CEC_{eff} values of the till samples. The prediction accuracy was assessed by the R^2 values from measured versus predicted CEC_{eff} values (Table 3, no. IV).

Results

Effect of Reduced Sample Masses of Effective Cation Exchange Capacity and pH Determination

The results of the sample mass Calibration Tests A and B (Fig. 1) showed that decreasing soil/solution ratios resulted in slightly

Table 3. Statistical relationships between effective cation exchange capacity (CEC_{eff}) data, complemental soil data, and diffuse reflectance infrared Fourier transform (DRIFT) spectra or single signal intensity at wave number 1246 cm^{-1}. All presented R^2 values were significant at the level of $P = 0.01$, except no. IV (= nonsignificant).

No.	Sample group and related measurement value†	Sample Set	Sample size (n)	Equation	R^2
I	linear regression, both sites: CEC_{eff} vs. mean clay content of bulk samples (i.e., horizons)	3	10	$y = 0.66x + 3.19$	0.91
II	calibration: PLSR for both sites: DRIFT spectra vs. CEC_{eff} (leave-one-out validation, measured vs. predicted)	2, 3 (loess, till)	20	$y = 1.01x + 0.07$	0.94
III	calibration: PLSR for loess samples: DRIFT spectra vs. CEC_{eff} (leave-one-out validation, measured vs. predicted)	2, 3 (loess)	11	$y = 0.61x + 7.56$	0.78
IV	validation of PLSR for loess samples by till samples	2, 3 (till)	9	$y = 1.23x - 1.40$	0.56
V	calibration: PLSR for till samples‡: DRIFT spectra vs. CEC_{eff} (leave-one-out validation, measured vs. predicted)	2, 3 (till)	8‡	$y = 0.61x + 4.67$	0.91
VI	validation of PLSR for till samples by loess samples	2, 3 (loess)	11	$y = 1.78x - 19.33$	0.76
VII	calibration: linear regression for both sites: CEC_{eff} measured vs. WN 1246 cm^{-1}	2, 3 (loess, till)	20	$y = 61896x + 4$	0.92
VIII	calibration: linear regression for loess samples: CEC_{eff} measured vs. WN 1246 cm^{-1}	2, 3 (loess)	11	$y = 65150x + 3$	0.94
IX	validation of linear regression for loess samples by till samples	2, 3 (till)	9	$y = 0.84x + 1.00$	0.85
X	calibration: linear regression for till samples: CEC_{eff} measured vs. WN 1246 cm^{-1}	2, 3 (till)	9	$y = 66000x + 4$	0.85
XI	validation of linear regression for till samples by loess samples	2, 3 (loess)	11	$y = 0.95x + 2.26$	0.94

† PLSR, partial least squares regression; WN, wave number.
‡ Without Cv (glacial till) sample (no. 15 in Table 2): the occurrence of carbonate peaks in this still not decalcified horizon (pH 7.67; Table 2) impeded the calculation of a clear relationship in the PLSR, at least when using this small sample size of $n = 9$. In contrast, when using the till samples for the validation of the loess model, the effect of the Cv (glacial till) sample was negligible.

higher CEC_{eff} values determined for smaller initial sample masses down to 0.6 g and in a strong CEC_{eff} decrease for masses <0.5 g. In contrast, the constant soil/solution ratio of Calibration Test B yielded constant CEC_{eff} values down to initial sample masses of 0.5 g. For initial sample masses of 2.0 and 2.5 g, the CEC_{eff} values differed between Calibration Tests A and B. At least for the samples of 2.5 g, this deviation must be attributed to the error of reproducibility between the two measurement series. However, in both Calibration Tests A and B, no considerable differences in the CEC_{eff} values were found between sample masses of 0.5 and 1.5 g ($n = 3$ for each test and sample mass). The sample mass calibration tests revealed that sample masses of 0.5 g were sufficient to determine the CEC_{eff} in soil samples. The extraction of exchangeable cations by constant soil/solution ratios (i.e., proportional to the original ratio) (Blakemore et al., 1987; ISO, 2018) was found to be the more appropriate method. Consequently, all presented results for Sample Sets 2 and 3 were obtained using initial sample masses of 0.5 g and the corresponding (i.e., proportionally smaller) solution volumes (Calibration Test B).

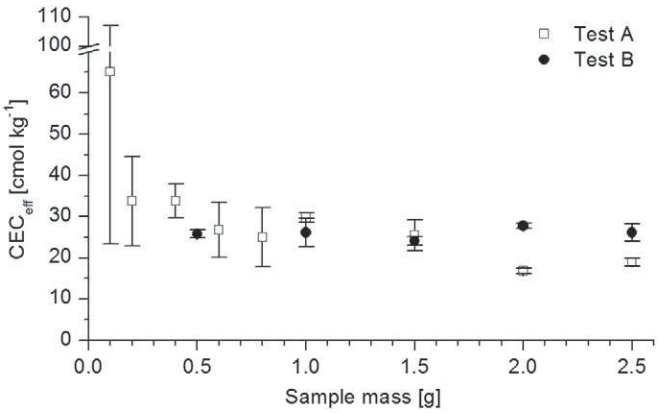

Fig. 1. Effective cation exchange capacity (CEC_{eff}) of bulk soil. Mean values (symbols) and SD (range bars) from the Bt horizon of a loess-derived Luvisol. Test A: constant $BaCl_2$ solution volume (i.e., decreasing soil/solution ratio). Test B: constant soil/solution ratio.

The pH calibration test (Fig. 2) showed negligibly small effects on the measured pH values when reducing the sample mass from 10 to 0.05 g and keeping the soil/solution ratio constant at 1:5. Even a change in the soil/solution ratio does not have a strong effect on the measured pH values, as Utermann (2004) showed.

Effective Cation Exchange Capacity of Bulk Samples and Separated Macropore Surfaces

The CEC_{eff} values of bulk and separated samples from loess-derived Luvisol (Sample Sets 2 and 3) were greater than those of the Luvisol developed from glacial till (Table 2). The CEC_{eff} values were linearly correlated (Table 3, no. I) with the mean clay contents of the soil horizons (Table 1). Regarding the soil horizons of each site, the Bt horizons revealed the highest CEC_{eff} values. Among the separated surfaces of different macropore types of the Bt horizons, the highest CEC_{eff} values were found for PIN, which were about 1.6 times (loess) and 2 times (till) higher than those of the Bt bulk samples (see column "CEC ratio" in Table 2). The lowest values of 70 and 85% of the CEC_{eff} of the Bt bulk samples were found for CS, EB, and EBcast; CS+C revealed increased CEC_{eff} values as compared with CS and EB, but these values were similar (loess) or only slightly higher (till) as compared with the Bt bulk samples. The difference between the CEC_{eff} of the Bt bulk soil and of CS+C and PIN material was greater for the till-Bt than

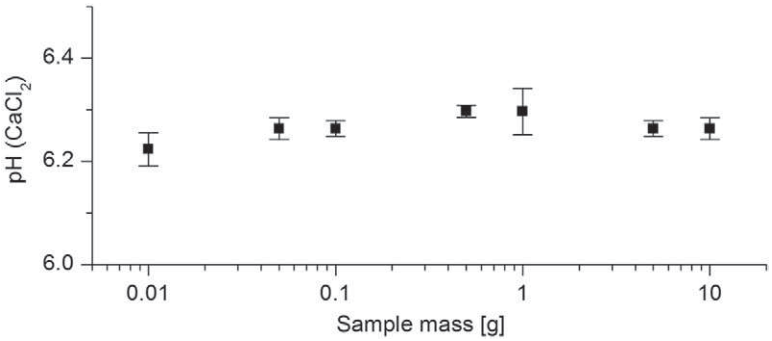

Fig. 2. The pH values of a bulk sample from a loess-derived Bt horizon vs. sample mass (logarithmic scale) for a constant soil/solution ratio; mean values (symbols) and SD (range bars) of each three repetitions.

for the loess Bt. The pH level of the till samples was higher than that of the loess samples. For each site, the pH values of PIN and CS+C were lower than those of CS and EB.

Relations between Cation Exchange Capacity and DRIFT Spectra

The PLSR showed a highly significant relationship (Table 3, no. II) between the DRIFT spectra and the corresponding CEC_{eff} values (Fig. 3a) considering DRIFT spectra from bulk soil samples and separated macropore surface material of the calibration data set (Sample Sets 2 and 3). In the PLSR model, most of the variance in the CEC_{eff} values of the samples was explained by two main components (Fig. 3b). Main Component 1 was primarily determined by loading values between WN 3800 and 3600 cm^{-1} (comprising O–H bonds of clay minerals), WN 2000 and 1800 cm^{-1} (lattice vibrations and overtones of Si–O groups), and ~1250 and 810 cm^{-1} (Si–O stretching of silicates and clay minerals) (Fig. 3c). Main Component 2 was primarily determined by loadings between WN 3500 and 3000 cm^{-1} (mainly O–H groups of adsorbed water), 2400 and 2100 cm^{-1} (assigned to base line shifts), 1800 and 1600 cm^{-1} (C=O, C=C, and N–H signals from SOM), ~1000 cm^{-1}, and <800 cm^{-1} (Si–O–Si and Si–O stretching). With respect to the main two components, the spectrum from the Ap1 horizon (no. 1) of the loess-derived Luvisol was very similar to the spectra of EB (no. 10), EBcast (no. 11), and CS (no. 7) of the Bt horizon as well as to spectra of the Bt-Cv horizon (no. 5) of the same site. Similarities between the Ap1 horizon (no. 12) and EBcast in the Bt horizon (no. 20) could also be found for the till-derived Luvisol. For the loess-Bt, DRIFT spectra of CS+C (no. 8) and in particular of PIN (no. 9) differed strongly from spectra of the other samples. For the till-Bt, spectra from PIN (no. 18) also differed strongly from those of the other samples, whereas only small differences were found between CS (no. 16) and CS+C (no. 17).

The PLSR calibrations for the single sites showed good relationships (Table 3, no. III and V). The PLSR model for the till samples also showed good prediction accuracy when validated by the loess data set (no. VI). In contrast, the validation of the PLSR for the loess samples was not as successful (no. IV). The calibration between the CEC_{eff} values and the normalized signal intensities at WN 1246 cm^{-1} (Fig. 4) revealed a strong linear relationship when considering both sites as well as the individual sites (Table 3, no. VII, VIII, and X). The validation of the relationship of one site by the data of the other site also showed good prediction accuracy (Table 3, no. IX and XI). In contrast to these results, no significant relationships were found between DRIFT spectra and corresponding pH values (L: $R^2 = 0.46$, T: $R^2 = 0.41$, and $R^2 = 0.28$ for all 20 samples from both sites). The correlation between WN 1246 cm^{-1} and the corresponding pH values was not significant, with $R^2 = 0.28$ for all 20 samples of both sites (L: $R^2 = 0.08$; T: $R^2 = 0.15$).

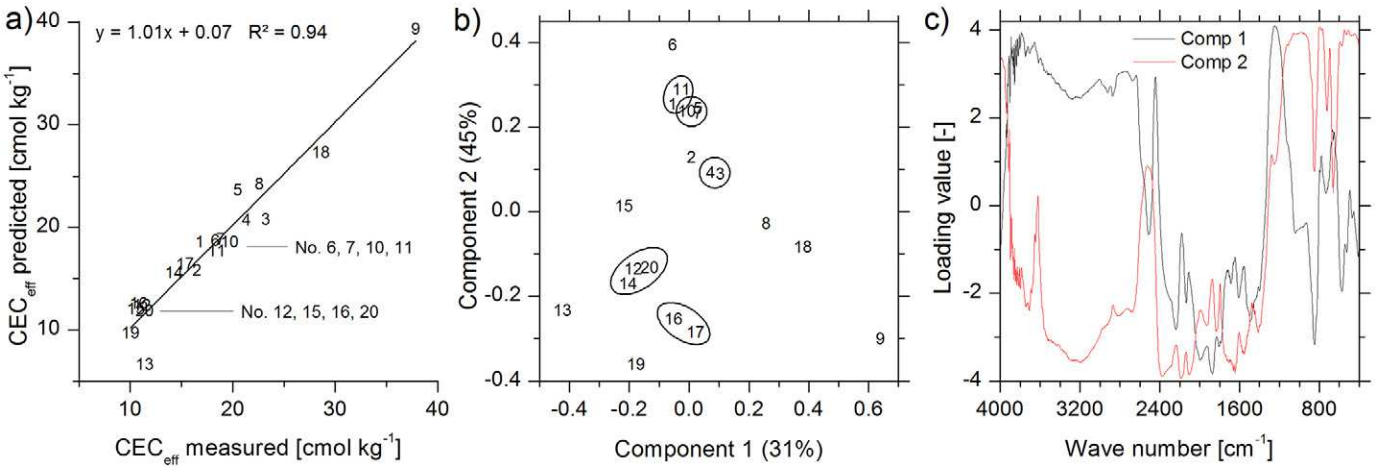

Fig. 3. Partial least squares regression between effective cation exchange capacity (CEC_{eff}) and normalized diffuse reflectance infrared Fourier transform spectra. (a) Prediction plot, (b) score plot for the two main components, and (c) wave number (WN) dependent loading values of these components (higher absolute loading values imply higher importance of the WN region; i.e., the infrared signal intensities on the components shown in the score plot). Sample numbers 1 to 11: loess; 12 to 20: glacial till. For number description see Table 2.

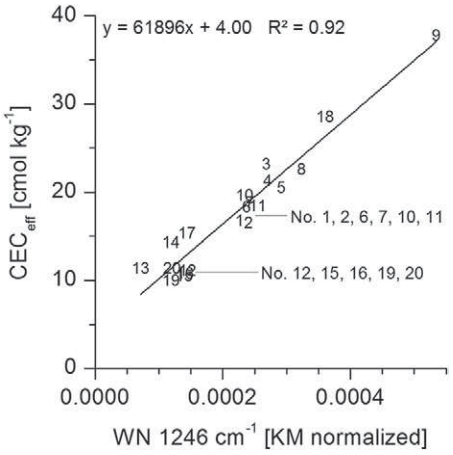

Fig. 4. Relation between normalized signal intensity at wave number (WN) 1246 cm^{-1} and effective cation exchange capacity (CEC_{eff}). Sample numbers 1 to 11: loess; 12 to 20: glacial till. For number description see Table 2.

Spatial Distribution of Effective Cation Exchange Capacity at Intact Macropore Surfaces

The spatial CEC_{eff} distribution at intact macropore surfaces was exemplarily predicted for a loess-derived sample (Fig. 5a) and a till-derived sample (Fig. 5d). Corresponding to the laboratory measurements (Table 2), the level of the predicted CEC_{eff} values of the loess sample was higher compared with that of the till sample. At intact macropore surfaces, the CEC_{eff} values predicted by the PLSR model (Fig. 3) ranged between 0 and 128 cmol kg^{-1} (L, Fig. 5b) and between 0 and 75 cmol kg^{-1} (T, Fig. 5e). Using the linear regression of the DRIFT signal intensity at WN 1246 cm^{-1} (Fig. 4), predicted CEC_{eff} values ranged between 15 and 45 cmol kg^{-1} (L, Fig. 5c) and between 10 and 39 cmol kg^{-1} (T, Fig. 5f). The highest CEC_{eff} values were found for the right-hand side EB of the loess sample (Fig. 5b) by both prediction methods. In the glacial till, the highest CEC_{eff} values were found for large pores filled with clayey material at the left, top-left, and bottom-right positions (Fig. 5e).

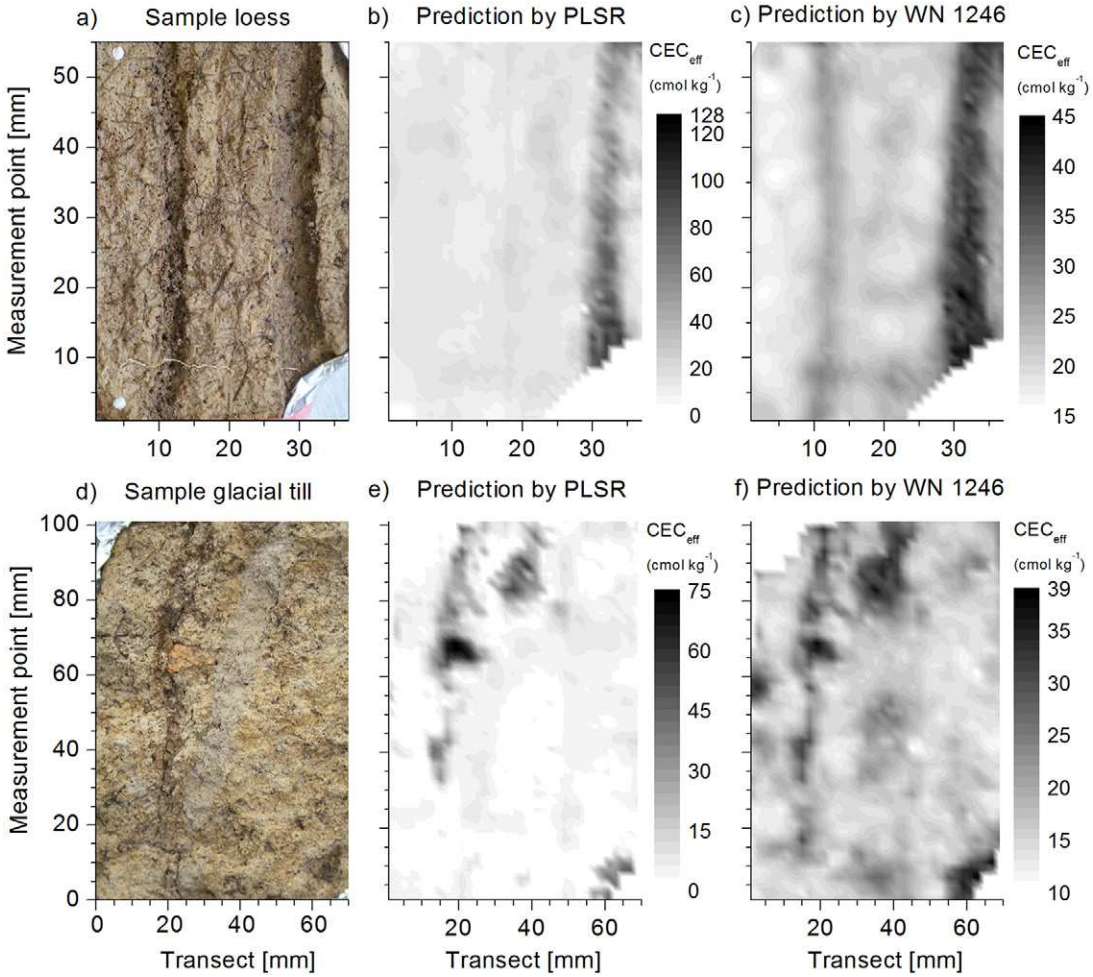

Fig. 5. (a) Photo of an intact sample surface from the loess-Bt showing crack surfaces with coated areas (darker structures) and two perpendicular earthworm burrows, (d) photo of an intact sample surface from the glacial till Bt horizon showing crack surfaces with coated areas (darker structures) and two perpendicularly orientated earthworm burrows, (b,e) maps of effective cation exchange capacity (CEC_{eff}) values predicted by partial least squares regression (PLSR) using the entire diffuse reflectance infrared Fourier transform spectra, and (c,f) maps of CEC_{eff} predicted by linear regression using the signal intensity at wave number (WN) 1246 cm^{-1}.

Discussion

Spatial Distribution of Effective Cation Exchange Capacity in Bt Horizons

The higher level of CEC_{eff} values in the loess-derived Luvisol reflected the higher mean clay content of this site in comparison to the till-derived Luvisol (Table 1). For each Luvisol, the highest CEC_{eff} values were found for the Bt horizons, which revealed the effect of clay migration from the topsoil (A horizons). The increased clay contents in the Bt horizon, as visible by clay coatings as a diagnostic feature in pedological description, and the correspondingly increased SOC contents of CS+C (Leue et al., 2018) contribute to the increased CEC_{eff} values to a great extent. This is underlined by similar levels of CS+C and bulk soil material (as expressed by CEC ratios near 1; Table 2). These findings are supported by the results of Keck et al. (2017), who measured the three-dimensional distribution of the CEC in soil cores with X-ray imaging and found that the X-ray image–derived CEC values (when averaged over the volume) correlated significantly with the CEC values of the bulk soil.

The PIN material revealed the highest CEC_{eff} values at each site (Table 2) and probably compensate for the smaller CEC_{eff} values of CS with respect to the CEC_{eff} of the entire Bt horizons (bulk samples). For PIN material (Samples 9 and 18), the value of the PLSR Main Component 1 (Fig. 3b) differed from those of the other separated samples. This indicated that the composition of the PIN material differs from the rest of the samples, in particular with respect to clay minerals and, in the case of the loess-Bt, organic functional groups such as C=O and C=C bonds, both of which were relevant for Component 1 of the PLSR. This emphasizes the relevance of clay minerals and SOM composition, in particular C=O groups (Kaiser et al., 2008), for the CEC_{eff} of soils.

The similarities in the DRIFT spectra composition with respect to the CEC_{eff} of the corresponding samples (Fig. 3b) found for EB, EBcast, and bulk soil material from the Ap horizons reflect the incorporation of organic-rich topsoil material by earthworms and was found earlier also with respect to SOC contents (Leue et al., 2018). The similarity of spectra from the loess-derived Ap and Bt-Cv horizons with those of the CS material (i.e., cracks from the Bt horizon without clay–organic coatings) illustrates the situation without the effect of clay migration and accumulation.

At the intact sample surfaces, the highest CEC_{eff} values, found for the right-hand side EB of the loess sample (Fig. 5b) seem to contradict the CEC_{eff} measurements of separated material (Table 2). We attribute such high CEC_{eff} values to the occurrence of pinhole fillings (with diameters <1 mm) and coating material along this EB wall. The coating material looked relatively similar to coatings found along cracks in this Bt horizon (Fig. 5a). Thus, the clear visual assignment of this macropore surface as EB, as indicated by a typical surface morphology as "channel," does not automatically imply macropore type–specific surface properties with respect to the organo-mineral composition and the resulting CEC_{eff} level of its surface.

Comparison of Statistical Techniques

Comparing the different methods calibration and prediction methods—PLSR and single WN 1246 cm^{-1}—we found that, despite different slopes and intercepts, the R^2 values of both methods were at the same level (Table 3). Also, the clustering of the samples (i.e., the spectra of the single-WN calibration; Fig. 4) was very similar to that of the PLSR prediction (Fig. 3a). For the signal at WN 1246 cm^{-1}, high slope values result from small absolute values after data (i.e., spectra) normalization.

The signal intensity at WN 1246 cm^{-1} is not attributed to one specific functional group. Located at a slope, its signal intensity is determined by those of the neighboring spectral regions. The latter ones are determined by functional groups from soil components important for the CEC and thus explain the high predictive power of WN 1246 cm^{-1}. The neighboring WN region 1353 to 1328 cm^{-1} is assigned to C=O, O–H, and N–O groups of SOM (Senesi et al., 2003; Spence and Kelleher, 2012); among those, C=O groups are relevant for the CEC (Kaiser et al., 2008). The other neighboring peak at WN 1160 cm^{-1} is assigned to Si–O stretching of silicates (Kumar and Rajkumar, 2014) such as clay minerals (phyllo-silicates). The wideness of these peaks in the DRIFT spectra is the reason that the signal intensities between these peaks do not decrease toward the baseline but build a slope between the two named regions. In comparison to the neighboring peaks, the signal at WN 1246 cm^{-1} was more strongly correlated with the CEC values measured in the calibration (Sample Sets 2 and 3).

The method of using the single-WN 1246 cm^{-1} seemed to predict a more differentiated spatial distribution of CEC_{eff} values for samples from both Luvisols (Fig. 5c and f). For example, the obviously older and partly filled EB at the left-hand side of the loess sample (Fig. 5a) showed slightly but clearly higher CEC_{eff} values than the surrounding crack surface. The same differentiation was found for the EB surface in the center of the till sample (visible as almost perpendicular linear; gray shape in Fig. 5d). In contrast, the PLSR model did not show increased CEC_{eff} values for these regions. The PLSR prediction values of the EB are in line with CEC_{eff} measurements, which revealed the same low level as found for uncoated cracks (Table 2). For these EB regions, the prediction by single WN seemed to slightly overestimate the CEC_{eff}. However, the PLSR prediction generally overestimates the CEC_{eff} values of the intact macropore surfaces by factors up to 3, compared with data obtained from separated samples (Table 2).

In contrast, the prediction by single WN provides a very plausible CEC_{eff} range, indicating that the calibration of CEC_{eff} values against one specific signal intensity (single WN) can be as appropriate as PLSR. This was underlined by better validation results of the linear regression using WN 1246 cm^{-1} (Table 3, no. IX and XI) in comparison to the validation of the PLSR (no. IV and VI), in particular in the case of the loess samples. This was not expected because the PLSR comprised the entire DRIFT spectra range of 3600 signal intensities (WNs 4000–400 cm^{-1}). The overestimation of CEC_{eff} values can be explained by differences between DRIFT spectra from separated samples (Sample Sets 2

and 3) and from intact surfaces (DRIFT mapping, Sample Set 1) as discussed in Leue et al. (2017). The effects of the sample surface geometry (Leue et al., 2011), particle size and arrangement (Leue et al., 2010a), and water residues may cause small baseline shifts and altered signal intensities of the DRIFT mapping spectra, which affect the prediction results of the PLSR (Leue et al., 2017).

Spatial Resolution

One immanent problem concerning the horizontal resolution of the presented approach is that a validation of the predictions from both methods by CEC_{eff} measurements at intact macropore surfaces ("ground truthing") is not possible. For validation, it would be necessary to separate the outermost surface from the area covered by the IR beam (here, diameter of ~1.5 mm) to assign the CEC_{eff} data obtained from this material to the respective DRIFT mapping spectra. The crucial point is that the amount of soil material separable from such a small surface area is too small for valid CEC_{eff} measurements. Leue et al. (2018) separated surface material from intact macropores in a 6.4- by 6.4-mm grid to map the spatial SOC distribution, yielding masses of ~1.5 to 2.0 mg per grid cell. Although these masses are sufficient for SOC analysis, they are not usable for valid CEC_{eff} determination, even with the method of reduced sample masses presented here. One possible solution for this problem could be the combination of different techniques, as described by Hapca et al. (2015), who used a combination of two-dimensional scanning electron microscope–energy-dispersive X-ray and three-dimensional X-ray computed tomography images to create three-dimensional maps of chemical soil characteristics at high resolutions.

Concerning the vertical resolution, the relationship between DRIFT spectra and CEC_{eff} values is probably affected by differences in the measurement depths. During DRIFT measurements, the IR beam penetrates the surface between a few micrometers and a few hundred micrometers (Fraser and Griffiths, 1990) up to a theoretical maximum of 1 to 2 mm (Moradi et al., 1998), as determined by the wavelength-dependent adsorption and scattering properties of the analyzed material (Ciani et al., 2005; Fraser and Griffiths, 1990). In contrast, the CEC determination by a batch method as used here comprises entire sample volumes that may not always have identical composition as compared with their outermost, intact sample surface covered by the IR beam.

Quantitative Relevance of Clay–Organic Coatings

Intact macropore surfaces from the two Luvisols investigated here contain significant amounts of highly condensed and aromatic SOM compounds, as determined by pyrolysis–field ionization mass spectrometry, which were related to the occurrence of clay (Leue et al., 2016, 2017). These compounds, including black carbon–like substances such as benzonitrile and naphthalene, consist of many C=O (and C=C) groups. To a great extent, the accumulation of these compounds has been attributed to preferential movement and deposition of burning residues (originating from straw combustion as frequently practiced in the past) along macropores in the Bt horizons, which were also preferential domains for clay mineral accumulation (Leue et al., 2016, 2017). The enrichment in C=O groups might also result from intensive oxidative microbial decomposition processes adding oxygen-bearing functional groups, such as –OH and –COOH. In combination with the small sizes, such SOM is highly associable with clay-sized minerals (Lehmann and Kleber, 2015). Independent of its origin, C=O groups are known to contribute to the CEC (Kaiser et al., 2008). The presented results suggest that increased CEC can be found at macropore surfaces with increased clay contents and associated contents of the aforementioned SOM compounds.

The measured and predicted CEC values of macropore surfaces are relatively high, but these high CECs are not likely to take effect in structured soils under field conditions because cation exchange between macropores and soil matrix physically depends on (i) the availability of different types of macropores (e.g., coated cracks and EBs) as preferential flow paths (e.g., Larsbo et al., 2016; Nobles et al., 2004), (ii) the soil moisture and possible repellency effects of organic matter along macropore surfaces (Haas et al., 2018; Leue et al., 2015; Lipsius and Mooney, 2006), and (iii) the hydraulic conductivity and consequently the percolation time (Hartmann et al., 1998). The CEC values presented here become relevant if (i) macropores are available, (ii) repellency effects are absent, and (iii) the percolation time is maximized (i.e., the water movement is retarded).

The quantitative effect of the clay–organic material of CS+C and PIN on the CEC_{eff} of the Bt horizons of both Luvisols is shown by the differences in CEC_{eff} of CS (representing the soil matrix) and the Bt-bulk soil sample (representing both the soil matrix and macropore surfaces) (Table 2). Resulting from clay migration, the Bt horizons of each Luvisol showed the highest CEC_{eff} values. Based on analyses of the organo-mineral composition (Leue et al., 2016, 2017), it can be assumed that the material of CS+C and PIN is nearly identical. Differences in the CEC_{eff} values between CS+C and PIN, as shown here, probably result from the manual separation of the crack coatings, which comprised the outermost coated surface as well as the underlying soil matrix, causing dilution effects (Leue et al., 2018). The similarity of both materials implies that crack coatings will principally have the same CEC_{eff} level as the pinhole material. In contrast, the material from EB and EBcast showed almost the same CEC_{eff} levels as determined for the uncoated cracks (Table 2). Thus, the effect of illuviated clay–organic material on the CEC_{eff} of the Bt horizons (BULK) could be roughly quantified from the weighted mean of the CEC_{eff} from uncoated cracks (i.e., soil matrix) and pinhole material.

$$a\mathrm{CEC}_{(\mathrm{CS-C})} + b\mathrm{CEC}_{(\mathrm{PIN})} = \mathrm{CEC}_{(\mathrm{BULK})} \quad [1]$$

where a and b are weighting factors, denoting the quantitative relevance (i.e., the volumes of the soil compartments).

Using

$$a = 1 - b \quad [2]$$

in Eq. [1] gives, for b:

$$b = \frac{CEC_{(BULK)} - CEC_{(CS-C)}}{CEC_{(PIN)} - CEC_{(CS-C)}} \quad [3]$$

Solving Eq. [3] with the CEC_{eff} data of the Bt horizons, the weighting factor b of the clay–organic material is 0.23 for the loess Bt and 0.20 for the till Bt. The calculation suggests that the clay–organic material found in crack coatings and pinholes contributes to ~20% of the CEC of the Bt horizons. This corresponds to the clay contents of the Bt horizons (Table 1). This calculation neglects differences in pore properties such as pore size distributions and macropore geometries of the Bt horizons, which are unknown to date but likely play an important role in the distribution of SOM along the pore wall and in the surrounding matrix (Quigley et al., 2018). However, it allows a rough estimation of volume proportion and the quantitative relevance of the illuviated clay–organic material with respect to total soil volume and the CEC_{eff} of the Bt horizons.

Conclusions

1. For the determination of CEC_{eff} values in small samples, as needed for predicting the two-dimensional spatial distribution of the CEC_{eff} at intact macropore surfaces, initial sample masses can be reduced to 0.5 g in the standard $BaCl_2$ batch method without a loss in accuracy. Conventional calibration of DRIFT spectra to CEC_{eff} values by a single specific DRIFT signal intensity that is determined by clay mineral as well as C=O of the SOM was able to yield an equally meaningful statistical relationship compared with PLSR. Thus, PLSR is not necessary in every case and can potentially be substituted by less complex statistical methods for predictions using infrared spectra. Differences in the predicted value levels and ranges between the predictions could not be evaluated due to a missing method of CEC_{eff} validation measurements along intact macropores at the millimeter to centimeter scale.
2. Independent of the prediction method, levels and spatial distribution of CEC_{eff} at macropore surfaces are strongly determined by the distribution of clay and associated SOM compounds, thereby underlining the relationships between clay minerals and/or C=O groups of SOM and CEC. The occurrence of clay coatings and pinhole fillings in parts of an EB suggests that physicochemical properties such as CEC_{eff} are not related to macropore morphology in every case. This might affect the assessment and modeling of such properties for soils and soil horizons.
3. The presented approach seems promising for quantifying CEC and further physicochemical properties of intact macropore surfaces as well as their effects on mass exchange and turnover. Future research on CEC or related parameters at intact macropore surfaces should focus on CEC determination in even smaller samples that correspond with the spatial resolution of DRIFT spectra to validate relations at millimeter-scaled coated surface areas of structured soils.

Acknowledgments

We thank Saskia Schiska and the central laboratory of the ZALF for the CEC_{eff} analyses; Sophie Godow, Ulrike Wypler, and Katja Knuhr for sample preparation; and Radka Kodešová and Miroslav Fér, Czech University of Life Sciences Prague, for support with the soil sampling in Hnevceves. This study was funded by the Deutsche Forschungsgemeinschaft (DFG), Bonn, Germany, under Grant LE 3177/1-2: "Quantification of small-scale physicochemical and microbiological properties of intact macropore surfaces in structured soils."

References

Abou Najm, M.R., J.D. Jabro, W.M. Iversen, R.H. Mohtar, and R.G. Evans. 2010. New method for the characterization of three-dimensional preferential flow paths in the field. Water Resour. Res. 46:W02503. doi:10.1029/2009WR008594

Alaoui, A., J. Lipiec, and H.H. Gerke. 2011. A review of the changes in the soil pore system due to soil deformation: A hydrodynamic perspective. Soil Tillage Res. 115–116:1–15. doi:10.1016/j.still.2011.06.002

Barton, C.D., and A.D. Karathanasis. 1997. Measuring cation exchange capacity and total exchangeable bases in batch and flow experiments. Soil Technol. 11:153–162. doi:10.1016/S0933-3630(97)00002-0

Blakemore, L.C., P.L. Searle, and B.K. Daly. 1987. Methods of chemical analysis of soils. New Zealand Soil Bureau Sci. Rep. 80. Dep. of Scientific and Industrial Research, Wellington, New Zealand.

Bundt, M., F. Widmer, M. Pesaro, J. Zeyer, and P. Blaser. 2001. Preferential flow paths: Biological 'hot spots' in soils. Soil Biol. Biochem. 33:729–738. doi:10.1016/S0038-0717(00)00218-2

Ciani, A., K.-U. Goss, and R.P. Schwarzenbach. 2005. Light penetration in soil and particulate minerals. Eur. J. Soil Sci. 56:561–574. doi:10.1111/j.1365-2389.2005.00688.x

Fér, M., M. Leue, R. Kodešová, H.H. Gerke, and R.H. Ellerbrock. 2016. Droplet infiltration dynamics and soil wettability related to soil organic matter of soil aggregate coatings and interiors. J. Hydrol. Hydromech. 64:111–120.

Fraser, D.J.J., and P.R. Griffiths. 1990. Effect of scattering coefficient on diffuse reflectance infrared spectra. Appl. Spectrosc. 44:193–199. doi:10.1366/0003702904085561

Gerke, H.H., and J.M. Köhne. 2002. Estimating hydraulic properties of soil aggregate skins from sorptivity and water retention. Soil Sci. Soc. Am. J. 66:26–36. doi:10.2136/sssaj2002.2600

Haas, C., H.H. Gerke, R.H. Ellerbrock, P.D. Hallet, and R. Horn. 2018. Relating soil organic matter composition to soil water repellency for soil biopore surfaces different in history from two Bt horizons of a Haplic Luvisol. Ecohydrology 11:e1949. doi:10.1002/eco.1949

Hapca, S., P.C. Baveye, C. Wilson, R.M. Lark, and W. Otten. 2015. Three-dimensional mapping of soil chemical characteristics at micrometric scale by combining 2D SEM-EDX data and 3D X-ray CT images. PLoS One 10(9):e0137205. doi:10.1371/journal.pone.0137205

Hartmann, A., W. Gräsle, and R. Horn. 1998. Cation exchange processes in structured soils at various hydraulic properties. Soil Tillage Res. 47:67–72. doi:10.1016/S0167-1987(98)00074-9

ISO. 2018. ISO Standard 12260. Soil quality: Determination of effective cation exchange capacity and base saturation level using barium chloride solution. ISO, Geneva, Switzerland.

IUSS Working Group WRB. 2006. World reference base for soil resources 2006. World Soil Resour. Rep. 103. FAO, Rome.

Janik, L.J., R.H. Merry, and J.O. Skjemstad. 1998. Can mid infrared diffuse reflectance analysis replace soil extractions? Aust. J. Exp. Agric. 38:681–696. doi:10.1071/EA97144

Jaremko, D., and D. Kalembasa. 2014. A comparison of methods for the determination of cation exchange capacity of soils. Ecol. Chem. Eng. S 21:487–498. doi:10.2478/eces-2014-0036

Jarvis, N.J. 2007. A review of non-equilibrium water flow and solute transport in soil macropores: Principles, controlling factors and consequences for water quality. Eur. J. Soil Sci. 58:523–546. doi:10.1111/j.1365-2389.2007.00915.x

Kaiser, M., R.H. Ellerbrock, and H.H. Gerke. 2008. Cation exchange capacity and composition of soluble soil organic matter fractions. Soil Sci. Soc. Am. J. 72:1278–1285. doi:10.2136/sssaj2007.0340

Kautz, T. 2015. Research on subsoil biopores and their functions in organically managed soils: A review. Renew. Agric. Food Syst. 30:318–327. doi:10.1017/S1742170513000549

Keck, H., B.W. Strobel, J.P. Gustafsson, and J. Koestel. 2017. Quantitative imaging of the 3-D distribution of cation adsorption sites in undisturbed soil. Soil 3:177–189. doi:10.5194/soil-3-177-2017

Kumar, R.S., and P. Rajkumar. 2014. Characterization of minerals in air dust particles in the state of Tamilnadu, India through FTIR, XRD and SEM analyses. Infrared Phys. Technol. 67:30–41. doi:10.1016/j.infrared.2014.06.002

Kuzyakov, Y., and E. Blagodatskaya. 2015. Microbial hotspots and hot moments in soil: Concept & review. Soil Biol. Biochem. 83:184–199. doi:10.1016/j.soilbio.2015.01.025

Larsbo, M., J. Koestel, T. Kätterer, and N. Jarvis. 2016. Preferential transport in macropores is reduced by soil organic carbon. Vadose Zone J. 15(9). doi:10.2136/vzj2016.03.0021

Lehmann, J., and M. Kleber. 2015. The contentious nature of soil organic matter. Nature 528:60–68. doi:10.1038/nature16069

Leue, M., K.-U. Eckhardt, R.H. Ellerbrock, H.H. Gerke, and P. Leinweber. 2016. Analyzing organic matter composition at intact biopore and crack surfaces by combining DRIFT spectroscopy and pyrolysis-field ionization mass spectrometry. J. Soil Sci. Plant Nutr. 179:5–17. doi:10.1002/jpln.201400620

Leue, M., K.-U. Eckhardt, H.H. Gerke, R.H. Ellerbrock, and P. Leinweber. 2017. Spatial distribution of organic matter compounds at intact macropore surfaces predicted by DRIFT spectroscopy. Vadose Zone J. 16(9). doi:10.2136/vzj2017.05.0111

Leue, M., R.H. Ellerbrock, D. Bänninger, and H.H. Gerke. 2010a. Impact of soil microstructure geometry on DRIFT spectra: Comparisons with beam trace modelling. Soil Sci. Soc. Am. J. 74:1976–1986. doi:10.2136/sssaj2009.0443

Leue, M., R.H. Ellerbrock, and H.H. Gerke. 2010b. DRIFT mapping of organic matter composition at intact soil aggregate surfaces. Vadose Zone J. 9:317–324. doi:10.2136/vzj2009.0101

Leue, M., H.H. Gerke, and R.H. Ellerbrock. 2011. Correcting microtopography effects on DRIFT mapping signals of organic matter at intact soil aggregate surfaces. Soil Sci. Soc. Am. J. 75:1626–1639. doi:10.2136/sssaj2010.0462

Leue, M., H.H. Gerke, and S.C. Godow. 2015. Droplet infiltration and organic matter composition of intact crack and biopore surfaces from clay-illuvial horizons. J. Plant Nutr. Soil Sci. 178:250–260. doi:10.1002/jpln.201400209

Leue, M., A. Wohld, and H.H. Gerke. 2018. Two-dimensional distribution of soil organic carbon at intact macropore surfaces in Bt-horizons. Soil Tillage Res. 176:1–9. doi:10.1016/j.still.2017.10.002

Lipsius, K., and S.J. Mooney. 2006. Using image analysis of tracer staining to examine the infiltration patterns in a water repellent contaminated sandy soil. Geoderma 136:865–875. doi:10.1016/j.geoderma.2006.06.005

Ludwig, B., F. Beese, and K. Michel. 2005. Modelling cation transport and pH buffering during unsaturated flow through intact subsoils. Eur. J. Soil Sci. 56:635–645. doi:10.1111/j.1365-2389.2005.00704.x

Madari, B.E., J.B. Reeves, P.L.O.A. Machado, C.M. Guimarães, E. Torres, and G.W. McCarty. 2006. Mid- and near-infrared spectroscopic assessment of soil compositional parameters and structural indices in two Ferralsols. Geoderma 136:245–259. doi:10.1016/j.geoderma.2006.03.026

Moradi, K., C. Depecker, J. Barbillat, and J. Corset. 1998. Diffuse reflectance infrared spectroscopy: An experimental measure and interpretation of the sample volume size involved in the light scattering process. Spectrochim. Acta A 55:43–64. doi:10.1016/S1386-1425(98)00163-2

Nobles, M.M., L.P. Wilding, and K.J. McInnes. 2004. Pathways of dye tracer movement through structured soils on a macroscopic scale. Soil Sci. 169:229–242. doi:10.1097/01.ss.0000126838.81093.20

Pagenkemper, S.K., M. Athmann, D. Uteau, T. Kautz, S. Peth, and R. Horn. 2015. The effect of earthworm activity on soil bioporosity investigated with X-ray computed tomography and endoscopy. Soil Tillage Res. 146:79–88. doi:10.1016/j.still.2014.05.007

Quigley, M.Y., W.C. Negassa, A.K. Guber, M.L. Rivers, and A.N. Kravchenko. 2018. Influence of pore characteristics on the fate and distribution of newly added carbon. Front. Environ. Sci. 13. doi:10.3389/fenvs.2018.00051

R Core Team. 2014. A language and environment for statistical computing. R Found. Stat. Comput., Vienna. http://www.R-project.org/ (accessed 1 Apr. 2015).

Ruiz, S., D. Or, and S.J. Schymanski. 2015. Soil penetration by earthworms and plant roots: Mechanical energetics of bioturbation of compacted soils. PLoS One [erratum: PLoS One doi:10.1371/journal.pone.0136225]. doi:10.1371/journal.pone.0128914

Senesi, N., V. D'Orazio, and G. Ricca. 2003. Humic acids in the first generation of EUROSOILS. Geoderma 116:325–344. doi:10.1016/S0016-7061(03)00107-1

Spence, A., and B.P. Kelleher. 2012. FT-IR spectroscopic analysis of kaolinite–microbial interactions. Vib. Spectrosc. 61:151–155. doi:10.1016/j.vibspec.2012.02.019

Utermann, J. 2004. Comparison of pH-measurements in soils according to ISO 10390 and DIN 19684-1. In: Handbook of forest analytics. Method A3.1.1.2, Appendix 1. Federal Ministry of Food and Agriculture, Bonn, Germany. p. 4–6.

Viscarra Rossel, R.A., D.J.J. Walvoort, A.B. McBratney, L.J. Janik, and J.O. Skjemstad. 2006. Visible, near infrared, mid infrared or combined diffuse reflectance spectroscopy for simultaneous assessment of various soil properties. Geoderma 131:59–75. doi:10.1016/j.geoderma.2005.03.007

Woche, S.K., M.-O. Goebel, R. Mikutta, C. Schurig, M. Kaestner, G. Guggenberger, and J. Bachmann. 2017. Soil wettability can be explained by the chemical composition of particle interfaces- An XPS study. Sci. Rep. 7:42877. doi:10.1038/srep42877